

---

# SPATIO-TEMPORAL JOINT ANALYSIS OF EXTREME OZONE AND MODERATE $PM_{2.5}$ IN CALIFORNIA WITH INLA APPROACH

---

**Jianan Pan<sup>1,2</sup> Kunyang He<sup>3</sup> Kai Wang<sup>3</sup> Qing Mu<sup>4</sup> Chengxiu Ling<sup>3\*</sup>**

<sup>1</sup> School of Mathematics and Physics, Xi'an Jiaotong-Liverpool University. 111 Ren'ai Road, Suzhou, China, 215123

<sup>2</sup> Department of Biostatistics, University of Washington. 1410 Northeast Campus Parkway, Seattle, WA, USA, 98105

<sup>3</sup> Academy of Pharmacy, Xi'an Jiaotong-Liverpool University. 111 Ren'ai Road, Suzhou, China, 215123

<sup>4</sup> Department of Health and Environmental Sciences, Xi'an Jiaotong-Liverpool University. 111 Ren'ai Road, Suzhou, China, 215123

\* Corresponding author: Chengxiu.Ling@xjtlu.edu.cn

## ABSTRACT

The substantial threat of concurrent air pollutants to public health is increasingly severe under climate change. To identify the common drivers and extent of spatio-temporal similarity of moderate  $PM_{2.5}$  and extreme ozone, this paper proposed a log Gaussian-Gumbel Bayesian hierarchical model allowing for sharing a SPDE-AR(1) spatio-temporal interaction structure. The proposed model outperforms in terms of estimation accuracy and prediction capacity for its increased parsimony and reduced uncertainty, especially for the shared ozone sub-model. Besides the consistently significant influence of temperature (positive), extreme drought (positive), fire burnt area (positive), and wind speed (negative) on both  $PM_{2.5}$  and ozone, surface pressure and GDP per capita (precipitation) demonstrate only positive associations with  $PM_{2.5}$

(ozone), while population density relates to neither. In addition, our results show the distinct spatio-temporal interactions and different seasonal patterns of  $PM_{2.5}$  and ozone, with peaks of  $PM_{2.5}$  and ozone in cold and hot seasons, respectively. Finally, with the aid of the excursion function, we see that the areas around the intersection of San Luis Obispo and Santa Barbara counties are likely to exceed the unhealthy ozone level for sensitive groups. Our findings provide new insights for regional and seasonal strategies in the co-control of  $PM_{2.5}$  and ozone. Our methodology is expected to be utilized when interest lies in multiple interrelated processes in the fields of environment and epidemiology.

**Keywords**  $PM_{2.5}$ - $O_3$  pollution, Bayesian joint hierarchical model, Sharing effect, Integrated nested Laplace approximation

## 1 Introduction

Fine particulate matter ( $PM_{2.5}$ ) and ozone ( $O_3$ ) are both critical pollutants with severe repercussions for global human health (Murray et al., 2020). The simultaneous presence is recognized as a significant public health concern, prompting extensive health-related investigations. In the United States, elevated ambient ozone levels are associated with increasing mortality rates (Hao et al., 2015), while long-term exposure to both  $PM_{2.5}$  and ozone pollution is linked to a higher risk of annual hospital admissions (Rhee et al., 2019). In north India, severe  $PM_{2.5}$  and ozone pollution are estimated to cause over 450,000 and 30,000 premature deaths annually, respectively (Karambelas et al., 2018). Despite rapid reductions (14.97%) in death caused by fine particular matter ( $PM_{2.5}$ ) in China from 2015 to 2020, those attributed to ozone increased by 94.61% during the same period

(Guan et al., 2021). Furthermore, long-term or short-term concurrent exposure to ozone and  $PM_{2.5}$  may lead to more severe health impacts compared to that for individual exposure (Siddika et al., 2019; Gold et al., 1999; Jerrett et al., 2013).

California, with an approximate population of 38,965,000 individuals, stands prominently among states grappling with severe air pollution, with six Californian cities in the top ten most polluted cities in terms of ozone and year-round particle pollution (American Lung Association, 2023). In addition, more than half counties (30 and 41 out of 58 counties respectively for ozone and  $PM_{2.5}$ ) in California are classified into counties with the most severe level of air pollution. The spatial disparity of air pollution including fine particulate matter,  $O_3$ , and  $NO_2$  and its positive relevance of health issues in California were identified by Jerrett et al. (2013). We refer to Meo et al. (2021); Mekonnen et al. (2021) for the positive association between worse air pollution and increased COVID-19 infection and mortality as well as preterm birth respectively. Additionally, a noticeable correlation has been discovered between both the immediate and prolonged impact of  $PM_{2.5}$  concentrations and the rise in mortality rates Shi et al. (2016), together with a remarkable increase in respiratory emergency department visits due to ozone exposure Malig et al. (2016). Given the serious  $O_3$  and  $PM_{2.5}$  in California, it is essential to identify its generation and spread to implement coordinated prevention and control measures (Huang et al., 2021; Kaufman et al., 2020). Bayesian spatio-temporal methods have been emphasized in air pollution investigations as it can help analyzing the hotspots of air pollution and incorporate both prior knowledge (e.g., neighbourhood information, the uncertainty of the regression coefficient) and available data, offering a comprehensive understanding of pollution patterns (Craig et al., 2008; Gardner-Frolick et al., 2022). For instance,  $PM_{2.5}$  and ozone pollution episodes in the U.S. are evidenced to be consistent with extreme weather phenomena such as heatwaves and wildfires in space and time (Schnell and Prather,

2017; Kalashnikov et al., 2022). Another advantage of Bayesian methods in the modelling of spatio-temporal data is that they can borrow strength from neighbouring areas to smooth the area-specific risks, and enable the statistical inference for missing data, measurement error, incompatible data and ecological bias (Weber et al., 2016; Beloconi et al., 2018; Zhou et al., 2020; Blangiardo et al., 2013). However, the complexity of the model and size of the database impose new challenges for using Bayesian methods through the Markov chain Monte Carlo (MCMC) algorithm. To this, the integrated nested Laplace approximation (INLA) approach has been developed as a computationally efficient alternative to MCMC with easy implementation using the R package (R-INLA package) (Rue et al., 2009). INLA is designed for latent Gaussian fields, including generalized linear mixed, spatial and spatio-temporal models, and have a great variety of applications (Cameletti et al., 2013; Koh et al., 2023; Chaudhuri et al., 2023; Opitz et al., 2020). Furthermore, INLA can be combined with the stochastic partial differential equation (SPDE) approach proposed by Lindgren et al. (2011) for incorporating spatial and spatio-temporal structure into point-reference data, which is widely used for air pollution evaluation (Cameletti et al., 2013; Villejo et al., 2023; Cameletti et al., 2019; Wang et al., 2023; Fioravanti et al., 2021)

In this study, we will employ Bayesian spatio-temporal methods to jointly analyse moderate  $PM_{2.5}$  and extreme ozone level. The co-pollution of  $PM_{2.5}$  and ozone has received increasing attention with emphasis on spatial and temporal patterns. Dai et al. (2021) focused on the correlation of daily average  $O_3$ - $PM_{2.5}$  in the Yangtze River Delta, China while Schnell and Prather (2017); Kalashnikov et al. (2022) showed extreme cluster of surface ozone, particulate matter, and temperature with consistent offsets in both space and time over eastern North America and U.S., respectively. However, there is no study on jointly spatio-temporal modelling for multiple pollutants but only a few research addressed this for  $PM_{2.5}$  (Wang et al., 2023) and ozone (De Hoogh et al., 2018)

separately. Note that public health risks and medical burden are more exacerbated by the long-term exposure of  $\text{PM}_{2.5}$  and severe ozone than the other cases (Vicedo-Cabrera et al., 2020). Therefore, we focus on monthly average of hourly  $\text{PM}_{2.5}$  concentration and monthly maxima of 8-hour maximum ozone from 181 stations in California from 2017 to 2021, based on the Air Quality Index (AQI) metric reported by the Environmental Protection Agency (EPA) in the United States. In addition, we consider to explore the influence of a series of variables on air pollution, namely, temperature, precipitation, wind speed, surface pressure, fire burnt area, extreme drought, GDP per capita and population density (Kinney, 2018; Jaffe and Wigder, 2012). The expected findings of spatio-temporal disparity of air pollution and its influential factors will help identify the hotspots for comprehensive co-regional risk management in California with air pollution exceeding the warning risk threshold via excursion function (Bolin and Lindgren, 2015), and raise awareness about the control of multiple air pollution patterns in terms of risk sources, human activities and climate environment.

The paper is organized as follows. In Section 2, we present the air quality data and the predictors. In Section 3, we establish the joint spatio-temporal Bayesian hierarchical models for examining the potential spatio-temporal shared pattern between  $\text{PM}_{2.5}$  and ozone. Model results are given in Section 4. We give an extensive discussion and conclusion in Section 5.

## **2 Data Description**

### **2.1 Air pollution data**

California is one of the wealthiest states located on the west coast of the U.S., making up of 58 counties spanning a geographical range with latitudinal and longitudinal coordinates of  $32^{\circ}30'N \sim$

$42^{\circ}N$  and  $114^{\circ}8'W \sim 124^{\circ}24'W$ . We obtained the air pollution dataset including hourly  $PM_{2.5}$

**Constrained refined Delaunay triangulation**

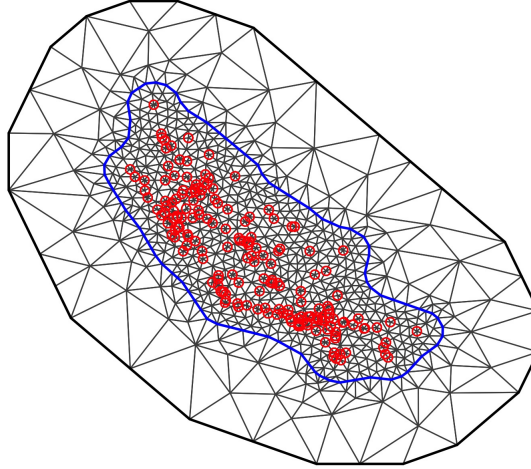


Figure 1: Mesh generated for Matérn covariance required in the SPDE approach, with 779 nodes. There are 181 stations in total with 92 stations for  $PM_{2.5}$  and 163 stations for ozone.

levels (with EPA parameter code: 88101, in  $\mu\text{g}/\text{m}^3$ ) collected by Federal Reference Method (FRM) or Federal Equivalent Method (FEM) observed from 92 weather stations and daily maximum 8-hour ground-level ozone (with EPA parameter code: 44201, in ppb) from 163 stations from 2017 to 2021, accessing the United States Environmental Protection Agency (EPA). The data is used to generate our response, the monthly mean of  $PM_{2.5}$  and the monthly maximum of  $O_3$  from the remaining 181 stations with more than 50% valid data in total.

We examined intuitively the temporal and spatial pattern of moderate  $PM_{2.5}$  and extreme ozone in Figs. 2 and 3. We see that  $O_3$  exhibits a conspicuous peak in the summer, while  $PM_{2.5}$  seems relatively high during autumn and winter. Meanwhile, according to the air quality category of the U.S. EPA, both  $PM_{2.5}$  (in  $\mu\text{g}/\text{m}^3$ ) and  $O_3$  (in ppb) can be grouped into six levels ( $PM_{2.5}$ : Good

(0–15.4), Moderate (15.5–40.4), Unhealthy for sensitive group (USG; 40.5–65.4), Unhealthy (65.5–150.4), Very Unhealthy (150.5–250.4) and Hazardous (250.5+) and O<sub>3</sub>: Good (0–54), Moderate (55–70), Unhealthy for Sensitive Groups (USG) (71–85), Unhealthy (86–105), Very Unhealthy (106–200), and Hazardous (201+)). From Fig. 2, PM<sub>2.5</sub> concentrations become relatively higher during cold seasons while ozone pollution becomes more serious in summer and autumn. Fig. 3 shows the spatial distribution of PM<sub>2.5</sub> in December and ozone in August during 2017–2021, California. Except 2019, noticeable PM<sub>2.5</sub> pollutants in many stations especially in the middle of California are observed at a Moderate or Unhealthy for Sensitive Groups (USG) level, while over 50% stations across California experienced serious ozone pollution at a USG or above level. These spatial and temporal variations of moderate PM<sub>2.5</sub> and extreme O<sub>3</sub> concentrations motivate us to incorporate spatial and temporal dependence into our Bayesian hierarchical modelling.

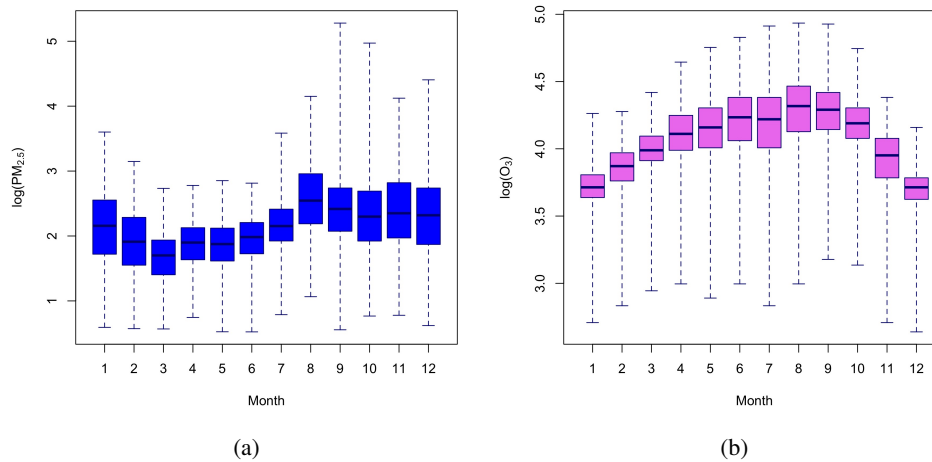


Figure 2: Boxplots of averaged monthly mean PM<sub>2.5</sub> concentrations (a) and averaged monthly maximum ozone levels (b) on log scale in California during 2017–2021.

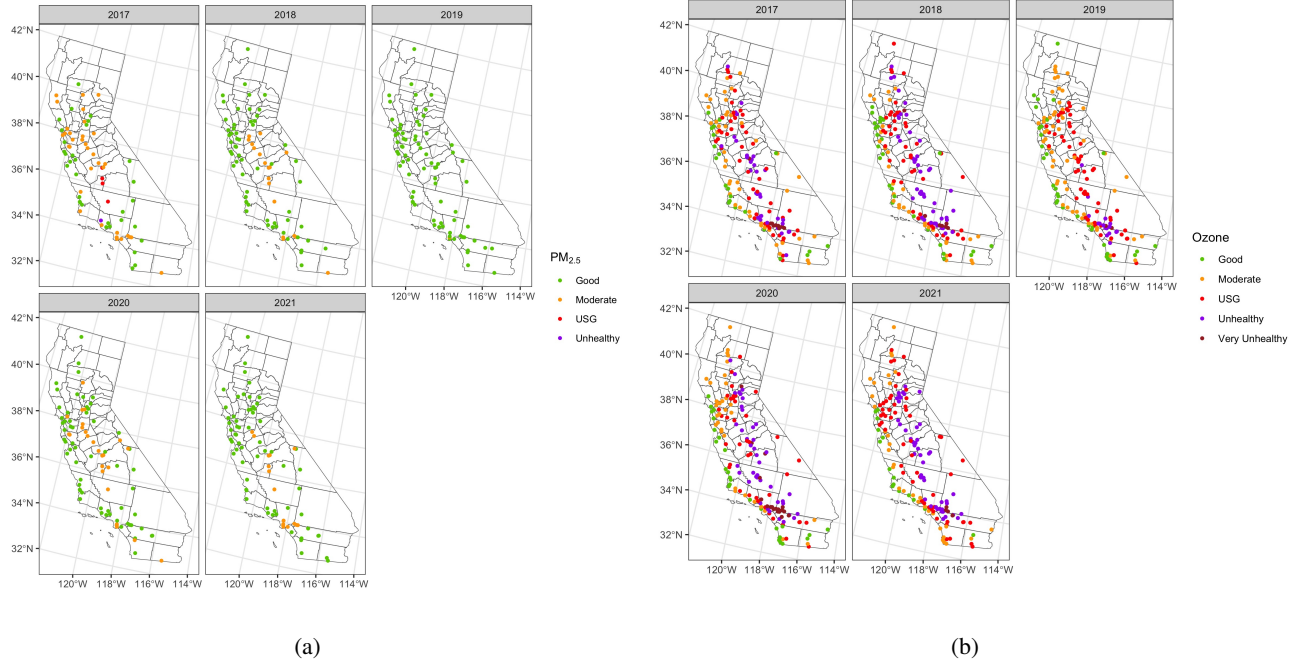


Figure 3: Spatial distribution of (a) monthly average of daily PM<sub>2.5</sub> concentrations (in  $\mu\text{g}/\text{m}^3$ ) in December, (b) monthly max 8-h ozone levels (in ppb) in August in each year during 2017–2021. Air quality category is given according to the EPA in the U.S.

## 2.2 Predictors

Table 1 lists air pollution variables together with 8 considered predictors. It consists of meteorological conditions (surface pressure, precipitation and wind speed), socio-economic factors (GDP per capita, population density), and other factors influencing the generation and spread of the pollutants (fire burnt area, extreme drought).

*Meteorological variables.* Given that climate and meteorological conditions may affect the generation and spread of air quality (Kinney, 2018), we collected surface pressure (hPa), precipitation (mm) and wind speed (10 m/s) from ERA5-Land dataset (Muñoz Sabater, 2019b), which is a reanalysis dataset containing variables on grids with resolution  $0.1^\circ \times 0.1^\circ$  over land surfaces, and monthly



average daily maximum temperature from ERA5 global atmospheric reanalysis (Muñoz Sabater, 2019a).

*Socioeconomic factors.* To incorporate the socioeconomic factors into account and reflect the influence of human activities, we collected annual GDP per capita (thousands of chained 2012 dollars) and annual population density (persons per square mile) in each county in California from Bureau of Economic Analysis (BEA), U.S. Department of Commerce, and United States Census Bureau.

*Other factors.* Noting that wildfire directly contributes to the generation of PM<sub>2.5</sub> and ozone (Jaffe and Wigder, 2012; O’Dell et al., 2019), and California is a state experiencing wildfire frequently during the summer and autumn (Li and Banerjee, 2021; O’Dell et al., 2019), we included fire burnt area representing the severity of the fire from the database provided by Service and Store (2019), captured at a grid scale of  $0.25^\circ \times 0.25^\circ$ . Drought is also an important aspect of the impact of climate change on air quality, associated with increased concentrations of ground-level ozone and PM<sub>2.5</sub> in the U.S. (Wang et al., 2017). We collected the weekly drought level from U.S. Drought Monitor by the National Drought Mitigation Center (NDMC), the U.S. Department of Agriculture (USDA) and the National Oceanic and Atmospheric Administration (NOA), which categorizes drought severity into six levels: Normal or wet conditions, Abnormally Dry (D0), Moderate Drought (D1), Severe Drought (D2), Extreme Drought (D3) to Exceptionally Drought (D4). **Each DM class is represented by one polygon saved in provided shape files.** We incorporate an extreme drought indicator at the monthly scale, with 1 if there is at least one week with extreme drought or above, and 0 otherwise. Noting that the aforementioned covariates are grid-specified (temperature, precipitation, surface pressure, wind speed, fire burnt area) or area specified (**extreme drought**, GDP per capita and

Table 1: Description of variables with its mean and standard deviation in parenthesis for continuous variables, and frequency for factor variables.

Variables (Unit)	Description	Range	Mean (Std)/Frequency	Resolution
PM <sub>2.5</sub> (µg/m <sup>3</sup> )	Monthly average PM <sub>2.5</sub> concentration on hourly basis	0.56 ~ 196.27	10.13(8.48)	station
Ozone (ppb)	Monthly maximum of daily maximum 8-hour ground-level ozone	14 ~ 139	59.93(17.38)	station
Temperature (°C)	Monthly average daily maximum temperature of air at 2m above the surface	-5.18 ~ 45.09	23.16(7.92)	0.1° × 0.1°
Precipitation (mm)	Monthly accumulated precipitation	0 ~ 22.67	1.41(2.43)	0.1° × 0.1°
Surface pressure (hPa)	Monthly average pressure of the atmosphere on the surface	730.60 ~ 1027.54	970.72(49.24)	0.1° × 0.1°
Wind speed (10m/s)	Horizontal wind speed	0 ~ 6.02	1.14(0.76)	0.1° × 0.1°
Fire burnt area (km <sup>2</sup> )	Total burnt area within each pixel per month	0 ~ 294.86	0.56(8.21)	0.25° × 0.25°
Extreme drought (dummy variable)	Indicator of extreme drought with 1 if at least one weekly drought level being D3 or D4 (extreme drought or above), and 0 otherwise	0,1	No. of 1's: 1573 No. of 0's: 9287	polygons in shape files
GDP (1000 USD per person)	Annual gross domestic product per person	27.06 ~ 247.13	55.39(27.68)	county
Population density (person per square miles)	Annual population density	1.753 ~ 18756.36	719.24(1584.68)	county

population density), we retrieved these datasets according to the coordinates of the stations which provided PM<sub>2.5</sub> and ozone in this study and matched them if the station's coordinate falls within the grid or area. In addition, we confirmed no multi-collinearity among the covariates included in Table 1 since all the Variance Inflation Factor (VIF) values are less than 5 (Salmeron et al., 2018). Note that the substantial dispersion in scales of the continuous predictors listed in Table 1, we standardize these variables to ensure their comparability in the following modelling analysis.

### 3 Modelling

#### 3.1 Spatio-temporal joint models

Let  $y_{\text{PM}}(s, t)$  and  $y_{\text{OZ}}(s, t)$  denote the logarithmic scales of monthly mean of PM<sub>2.5</sub> and monthly maximum of O<sub>3</sub> at location  $s \in \mathcal{S}$  and time  $t \in \mathcal{T}$ , where  $\mathcal{S}$  represents the study area containing 181 meteorological stations in California and  $\mathcal{T} = \{1, 2, \dots, 60\}$  denotes the study period (2017–2021).

We establish the following joint spatio-temporal models with mixed effects:

$$\begin{aligned}
 [y_{\text{PM}}(\mathbf{s}, t) \mid \mu_{\text{PM}}(\mathbf{s}, t), \sigma_{\text{PM}}] &\sim \text{Gaussian}(\mu_{\text{PM}}(\mathbf{s}, t), \sigma_{\text{PM}}), \\
 [y_{\text{OZ}}(\mathbf{s}, t) \mid \mu_{\text{OZ}}(\mathbf{s}, t), \sigma_{\text{OZ}}] &\sim \text{Gumbel}(\mu_{\text{OZ}}(\mathbf{s}, t), \sigma_{\text{OZ}})
 \end{aligned} \tag{1}$$

with

$$\mu_{\text{PM}}(\mathbf{s}, t) = \mathbf{x}(\mathbf{s}, t)^\top \boldsymbol{\beta}_{\text{PM}} + f_1(\mathbf{s}, t) + \epsilon_1(\mathbf{s}, t), \quad (2)$$

$$\mu_{\text{OZ}}(\mathbf{s}, t) = \mathbf{x}(\mathbf{s}, t)^\top \boldsymbol{\beta}_{\text{OZ}} + f_2(\mathbf{s}, t) + \epsilon_2(\mathbf{s}, t).$$

As shown in Eq.(1), we suppose that the logarithmic scales of moderate  $\text{PM}_{2.5}$  and extreme  $\text{O}_3$  follow respectively Gaussian and Gumbel distributions (the generalized extreme value (GEV) distribution with  $\xi = 0$ ), respectively (Wang et al., 2023; Blangiardo et al., 2013). The Gumbel distribution is often well-suited for modelling extreme events (block maxima) in environmental studies, such as abnormal precipitation, earthquakes and air quality (Rulfova et al., 2016; Pisarenko et al., 2014; Shcherbakov et al., 2019; Martins et al., 2017).

With regard to the spatio-temporal variability of  $\text{PM}_{2.5}$  and  $\text{O}_3$ , we allow the location parameter  $(\mu_{\text{PM}}, \mu_{\text{OZ}})$  in our model (see Eq.(2)) to vary according to a combination of fixed effects  $(\boldsymbol{\beta}_{\text{PM}}, \boldsymbol{\beta}_{\text{OZ}})$ , random effects  $(f_1, f_2)$ , and an independent, mean zero Gaussian measurement error  $(\epsilon_1, \epsilon_2)$  with precision  $(\tau_1, \tau_2)$ . Here, both fixed effects are associated with the predictor vector  $\mathbf{x}(\mathbf{s}, t)$ , consisting of the intercept, temperature, precipitation, surface pressure, wind speed, fire burnt area, extreme drought, GDP per capita and population density.

In the following, we specify the random effects  $(f_1, f_2)$  in Eq.(1) to interpret the spatial and temporal variability in the residuals of  $\text{PM}_{2.5}$  and  $\text{O}_3$  after adjusting for the influences of the fixed effects and measurement error.

**Model 1. With only fixed effects and measurement errors.** Consider model in Eq.(1) without any other spatial or temporal effects, namely with both  $f_1$  and  $f_2$  equal zero. In other words, we model  $\text{PM}_{2.5}$  and  $\text{O}_3$  separately, with only fixed effects associated with predictors and measurement error. We take this as a reference model to compare the model performance in estimation and prediction.

**Model 2. With sharing spatial and temporal random effect.** Let  $y(t)$  and  $m(t)$  represent the year and month at time  $t$ , respectively, i.e.,  $y(t) \in \{1, 2, 3, 4, 5\}$  counting the year from 2017 to 2021 and  $m(t) \in \{1, 2, \dots, 12\}$  counting the month of the year.

$$f_1(\mathbf{s}, t) = u_1(\mathbf{s}) + u_2(m(t)) + u_3(y(t)),$$

$$f_2(\mathbf{s}, t) = \beta_1 u_1(\mathbf{s}) + \beta_2 u_2(m(t)) + \beta_3 u_3(y(t)) + u'_1(\mathbf{s}).$$

The spatial random effect ( $u_1$ ) and the temporal random effects ( $u_2, u_3$ ) are shared between the submodels with scales  $\beta_i, i = 1, 2, 3$ . The sharing components allow us to model the effects that jointly affect both PM<sub>2.5</sub> and O<sub>3</sub> levels. This approach increases model parsimony and reduces the uncertainty in estimating these effects, particularly when observed responses provide insufficient information for complex predictive structures. The scaling factor  $\beta_i$  also provides some insights into the joint drivers, highlighting the extent of similarities of the spatial and temporal effects in the two processes. Besides the sharing effects, we include an additional spatial term  $u'_1$  to capture the extra effect in the O<sub>3</sub> sub-model. Both the spatial effects  $u_1, u'_1$  are structured by the SPDE approach with a mesh (Fig. 1 constructed with guidance in Righetto et al. (2020)). For example, we suppose that  $u_1(\mathbf{s}), \mathbf{s} \in \mathcal{S}$  a continuous-time Gaussian random field with Matérn covariance structure: For two locations  $s_i$  and  $s_j$ , we have (Cameletti et al., 2013)

$$\text{Cov}(u_1(s_i), u_1(s_j)) = \frac{\sigma^2}{2^{\nu-1}\Gamma(\nu)} \left( \sqrt{8\nu} \frac{h}{\rho} \right)^\nu K_\nu \left( \sqrt{8\nu} \frac{h}{\rho} \right),$$

where  $h$  denotes the Euclidean distance between  $s_i$  and  $s_j$ ,  $\Gamma$  is the gamma function,  $K_\nu$  is the modified Bessel function of the second kind,  $\rho > 0$  is the range parameter which denotes the range of non-negligible spatial dependence,  $\nu > 0$  is the smoothness parameter, and  $\sigma^2 > 0$  is the

marginal variance.

Meanwhile, the temporal effects  $u_2, u_3$  follow the first-order autoregression process (AR(1)), i.e.,

$$u_2(m(t)) = a_m u_2(m(t) - 1) + \epsilon_t^m, \quad u_3(y(t)) = a_y u_3(y(t) - 1) + \epsilon_t^y$$

with  $\epsilon_t^m$  and  $\epsilon_t^y$  being Gaussian white noise with variance  $\sigma_m^2$  and  $\sigma_y^2$ , respectively. In addition, we restrict the temporal effect for month ( $u_2$ ) to satisfy the cyclic condition which modified the graph so that the last node ( $m(t) = 12$ ) is a neighbour of both  $m(t) = 11$  and  $m(t) = 1$ .

**Model 3. With sharing spatio-temporal random effect.** We incorporate the SPDE spatial effect and monthly temporal effects into an SPDE-AR(1) model (Cameletti et al., 2013). Compared with Model 2, we combined the SPDE spatial random effect and the monthly temporal effect as follows.

$$f_1(\mathbf{s}, t) = u_4(y(t)) + u_5(\mathbf{s}, m(t)),$$

$$f_2(\mathbf{s}, t) = \beta_4 u_4(y(t)) + \beta_5 u_5(\mathbf{s}, m(t)) + u_5'(\mathbf{s}, m(t)).$$

Here  $u_4$  is the yearly AR(1) model similar to  $u_3$  in Model 2. The spatio-temporal random effect  $u_5(\mathbf{s}, m(t))$  follows a SPDE-AR(1) model proposed by Cameletti et al. (2013). In particular,

$$u_5(\mathbf{s}, m(t)) = a_s u_5(\mathbf{s}, m(t) - 1) + w(\mathbf{s}, m(t)),$$

$$w(\mathbf{s}, m(t)) \sim \mathcal{GP}_{2D-SPDE}(\rho_s, \sigma_s, \nu_s).$$

We see that the  $u_5$  varies in time via a monthly cyclic AR(1) model over a year with coefficient  $a_s$  and its innovation part  $w(\mathbf{s}, m(t))$  follows a two-dimensional SPDE model in space and independent at different time points (Lindgren et al., 2011). Similar to Model 2, the additional term  $u_5'(\mathbf{s}, m(t))$  has the same SPDE-AR(1) structure as  $u_5$ . While the sharing coefficient  $\beta_5$  reveals the similar/inverse

spatiotemporal effect between the two processes, the additional term  $u'_5$  increases both model fitness and credibility of inference.

### 3.2 Prior definition

A typical property of Bayesian inference is that the prior distribution is required during the calculation of posterior density. We define vague Gaussian priors for the fixed effects  $\beta_{\text{PM}}, \beta_{\text{OZ}}$ , the sharing coefficients  $\beta_i, i = 1, \dots, 5$ , and the variance parameters  $\sigma_m^2, \sigma_y^2$  in the AR(1) temporal model. Note that INLA often defines the precision parameter with  $\tau = 1/\sigma^2$ , we set log-gamma priors for  $\tau_{\text{PM}}$  (in Gaussian likelihood),  $\tau_{\text{OZ}}$  (in Gumbel likelihood) as well as  $\tau_1, \tau_2$  in the measurement errors. The smooth parameter in the SPDE approach is commonly fixed with  $\nu_s = 1$  in spatial analysis. For other parameters, we employ the penalized complexity (PC) priors (Simpson et al., 2017) that penalize the complex models to avoid overfitness. Following the relevant research (Fuglstad et al., 2019), the PC priors for the SPDE and SPDE-AR(1) processes are defined with  $\text{Prob}(\rho_s < 10) = 0.9, \text{Prob}(\sigma_s > 0.5) = 0.1$ , which means the spatial dependence is unignorable within the range of 10km and the probability of the standard deviation larger than 0.5 is very low. For the AR(1) models, we set  $\text{Prob}(a_s > 0) = 0.95$  for the SPDE-AR(1) model and  $\text{Prob}(a_m > 0) = \text{Prob}(a_y > 0) = 0.95$  for other monthly and yearly AR(1) models. The sensitivity analysis utilized default priors in INLA and varied spatial nodes in the SPDE approach. The results confirm the robustness of all the priors we defined, with consistent posterior estimations of fixed effects and parameters.

## 4 Results

### 4.1 Model comparison

We carried out the three joint models proposed in Section 3.1 through the implementation of INLA. The performance of the model's estimation on the training set (2017–2020) and prediction on the validation set (2021) is compared. Model performance on the training set is assessed using the Watanabe-Akaike information criterion (WAIC; Watanabe, 2010), deviance information criterion (DIC; Spiegelhalter et al., 2002), and the conditional predictive ordinate (CPO; Lewis et al., 2014) with its summative form of logarithm score (LS; Gneiting and Raftery, 2007). For the validation set, we utilize the correlation coefficient to measure the linear correlation between predicted and observed values, and the root mean square error (RMSE) for the magnitude of its difference, and introduce scaled threshold weighted continuous ranked probability score (StwCRPS; Bolin and Wallin, 2023; Vandeskog et al., 2022) to evaluate the model predictive power in the tail parts, namely the model fitness of extreme  $O_3$ . All the criteria except the correlation exhibit preferences for lower values.

The evaluation of the performance is shown in Table 2. On the training set, Model 3 exhibits superior performance with lower DIC, WAIC and LS. The validation for  $PM_{2.5}$  and  $O_3$  is evaluated separately. All three  $O_3$  sub-models perform better than the  $PM_{2.5}$  models, achieving correlations over 70% and RMSE below 0.20. This can be attributed to the availability of  $O_3$  data, enhancing the reliability of  $O_3$  prediction. Despite Model 3 failing to excel in StwCRPS on the  $O_3$  validation set, the performance is favourable in both correlation and RMSE, and it is still selected as the optimal model for the subsequent analysis.

Fig. 4 shows the performance of Model 3 concerning its accuracy of model estimates (on the training set) and predictions (on the validation set). Compared with the  $PM_{2.5}$  sub-figures, the scatters in  $O_3$  sub-figures are clustered more closely around the identity line, indicating a stronger alignment between observed and estimated values. The  $PM_{2.5}$  sub-model successfully captures overall trends but spreads out at the right tail (large values), aligning with the larger RMSE compared to the  $O_3$  model.

Table 2: Model comparison for performance on the training and validation sets with different random effects specified in Models 1  $\sim$  3. A higher correlation and lower values in all other criteria indicate better fitness.

Model	Training Set (2017-2020)			PM <sub>2.5</sub> Validation Set (2021)		O <sub>3</sub> Validation Set (2021)		
	DIC	WAIC	LS	Correlation	RMSE	Correlation	RMSE	StwCRPS ( $p = 0.7$ )
Model 1	43.33	3045.74	135169.72	0.39	0.52	0.74	0.20	0.35
Model 2	-4179.99	-3003.04	119478.76	0.54	0.46	0.87	0.14	3.12
Model 3	-9863.06	-8608.15	102963.23	0.78	0.34	0.90	0.13	6.52

## 4.2 Summary and prediction

Based on the optimal model (Model 3 with SPDE-AR(1) random effect), we summarized the posterior mean of fixed effects associated with all predictors (Table 1) together with its 95% posterior credible interval (CI) in Table 3 with visualization in Fig. 5. The common drivers of  $PM_{2.5}$  and ozone were identified, including temperature (positive association), extreme drought (positive), fire burnt area (positive), wind speed (negative association), and precipitation (both surface pressure and GDP per capita) shows only significant influence on ozone ( $PM_{2.5}$ ), while population density affects neither. This observation suggests that human activities might not be as dominant in influencing air pollution compared to environmental processes (Wang et al., 2020). Specifically, with one unit standard deviation ( $23.16^\circ C$ ) increase of temperature, monthly average  $PM_{2.5}$  and maximum  $O_3$  are expected to increase by 80% (95% CI: 68%, 92%) and 22% (95% CI:



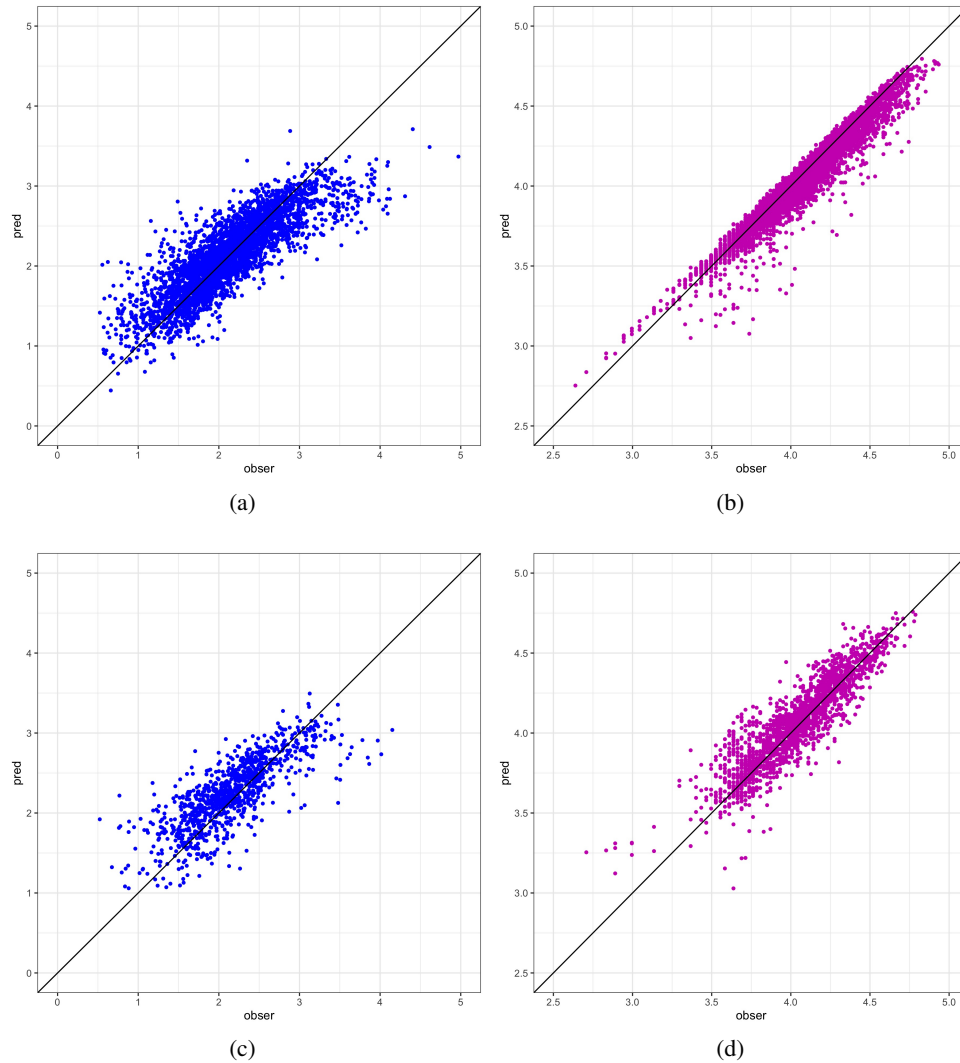


Figure 4: Visualisation of model prediction capability for PM<sub>2.5</sub> in (a,c) and ozone in (b,d). Here (a,b) are for training sets in 2017–2020, and (c,d) for testing sets in 2021. Model with points distributed along the identity line indicates the better one.

20%, 24%), respectively. In addition,  $PM_{2.5}$  and ozone in extreme drought month are expected to increase by a factor of 1.11 (95% CI: 1.03, 1.20) and 1.041 (95% CI: 1.026, 1.056), respectively. Meanwhile, the station located within a severe fire burnt area tends to have severe air pollutants, with 1.05 (95% CI: 1.04, 1.06) in  $PM_{2.5}$  and 1.005 (95% CI: 1.003, 1.007) in  $O_3$  times inclines with every  $0.56 \text{ km}^2$  increase of monthly cumulative burnt area, which suggests a direct connection between fire severity and air pollution. All the positive findings are consistent with the analysis of heatwaves in Schnell and Prather (2017), drought in Wang et al. (2017) and wildfire in Kalashnikov et al. (2022). In contrast, wind speed shows a significantly negative relationship with a decline by 3% (95% CI: 0.4%, 5.6%) in mean  $PM_{2.5}$  and 1.48% (95% CI: 0.89%, 2.08%) in max  $O_3$ . for every 11.4m/s increase of monthly averaged wind speed, coinciding with the fact that the higher concentration is caused by stagnant winds limiting the horizontal dispersion of pollutants (Kinney, 2018). Finally, it is noted that surface pressure and precipitation are only positively associated with  $PM_{2.5}$  and ozone, respectively. Our result of positive association between precipitation- $O_3$  is in consistency with that found by Arshinova et al. (2019). There are still some other studies showing the inverse (negative) impacts of precipitation on ozone (Cao and Yin, 2020; Liu et al., 2019).

Table 3: Posterior mean (95% credible interval) of the fixed effects.

Covariate	Month mean model ( $\beta_{PM}$ )		Month maxima model ( $\beta_{OZ}$ )	
	Mean	95% CI	Mean	95% CI
Temperature	0.588	(0.522, 0.654)	0.199	(0.186, 0.212)
Precipitation	0.011	(-0.010, 0.031)	0.021	(0.017, 0.025)
Surface pressure	0.165	(0.041, 0.290)	-0.026	(-0.065, 0.014)
Wind speed	-0.031	(-0.058, -0.004)	-0.015	(-0.021, -0.009)
Fire burnt area	0.051	(0.041, 0.062)	0.005	(0.003, 0.007)
Extreme drought	0.103	(0.025, 0.180)	0.040	(0.026, 0.055)
GDP per capita	0.065	(0.004, 0.126)	0.024	(-0.002, 0.050)
Population density	-0.015	(-0.054, 0.025)	-0.020	(-0.062, 0.023)

The posterior means, standard deviations, and 95% credible intervals of parameters are presented in Table 4. The posterior mean of the range parameter  $\rho_s$  is 2.92 (95% CI: 2.56, 3.37) in the

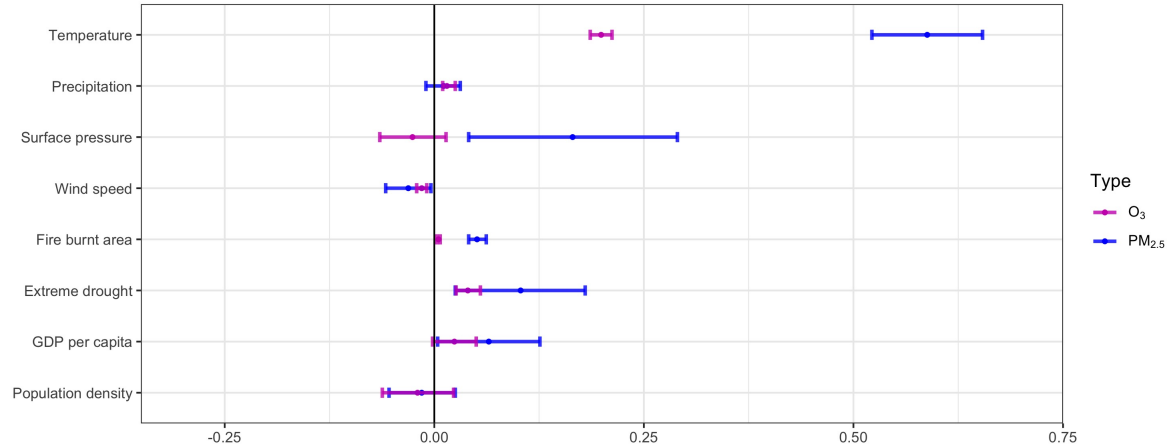


Figure 5: Fixed effect quantiles plot. The three nodes in the quantiles plot indicate 0.025 quantile, mean and 0.975 quantile of the posterior estimates of each fixed effect associated with all predictors in Model 3.

sharing SPDE-AR(1) model and  $\rho'_s$  is 2.85 (95% CI: 2.46, 3.28) in the additional model. Both range parameters are significantly below 10, which is aligned with the PC prior and implies that spatial dependence is even weaker. The auto-correlation coefficients  $a_s$ ,  $a'_s$ ,  $a_y$  are estimated as 0.91, 0.98 and 0.56, respectively. This indicates strong inner-annual and inter-annual dependence, aligning with the temporal trends presented in the box-plot (Fig. 2). More importantly, the coefficient ( $\beta_5$ ) for sharing SPDE-AR(1) term is significantly negative with value  $-0.708$  (95% CI:  $-0.896$ ,  $-0.476$ ), suggesting an inverse sharing of the spatio-temporal effect between moderate PM<sub>2.5</sub> and extreme O<sub>3</sub> processes. This evidence coincides with the findings of the enhanced PM<sub>2.5</sub> levels suppress surface solar radiation and could weaken O<sub>3</sub> production with the low diurnal peaks (Jia et al., 2017).

Based on Model 3 in the training set (2017–2020), Fig. 6 presents the prediction of PM<sub>2.5</sub> and ozone across the entire state of California for each month in 2021. Generally, the concerns regarding PM<sub>2.5</sub> are more noticeable in August, September, November and December. Conversely, monthly maximums of ozone peak in hot seasons, specifically from April to September. These inverse temporal variation patterns of air pollutants align with our empirical analysis (Fig. 2). Regarding

Table 4: Posterior estimates of mean, standard deviation and quantiles of the parameters. The precision of Gaussian ( $\tau_{PM}$ ) and Gumbel distributions ( $\tau_{OZ}$ ), the range parameter ( $\rho_s$ ), the standard deviation ( $\sigma_s$ ) and the autocorrelation coefficients ( $a_s$ ) in the sharing SPDE-AR(1) model, ( $\rho'_s, \sigma'_s, a'_s$ ) in the extra SPDE-AR(1) model, precision ( $\tau_y$ ) and autocorrelation coefficient ( $a_y$ ) in the yearly AR(1) model, precision of measurement errors ( $\tau_1, \tau_2$ ), and sharing effect coefficients ( $\beta_4, \beta_5$ ).

Parameter	Mean	Stdev	0.025 quantile	0.5 quantile	0.975 quantile
$\tau_{PM}$	8.466	0.185	8.081	8.470	8.817
$\tau_{OZ}$	212.865	7.673	197.160	213.067	227.423
$\rho_s$	2.917	0.204	2.557	2.903	3.370
$\sigma_s$	0.618	0.030	0.565	0.616	0.685
$a_s$	0.907	0.009	0.891	0.907	0.925
$\rho'_s$	2.851	0.202	2.457	2.845	3.283
$\sigma'_s$	0.461	0.029	0.405	0.460	0.522
$a'_s$	0.976	0.002	0.971	0.976	0.981
$\tau_y$	43.959	7.083	31.112	43.575	59.077
$a_y$	0.561	0.039	0.476	0.563	0.631
$\tau_1$	1276.212	108.649	1097.029	1266.046	1528.065
$\tau_2$	309.929	16.141	281.197	308.852	344.901
$\beta_4$	0.005	0.017	-0.027	0.005	0.039
$\beta_5$	-0.708	0.107	-0.898	-0.714	-0.476

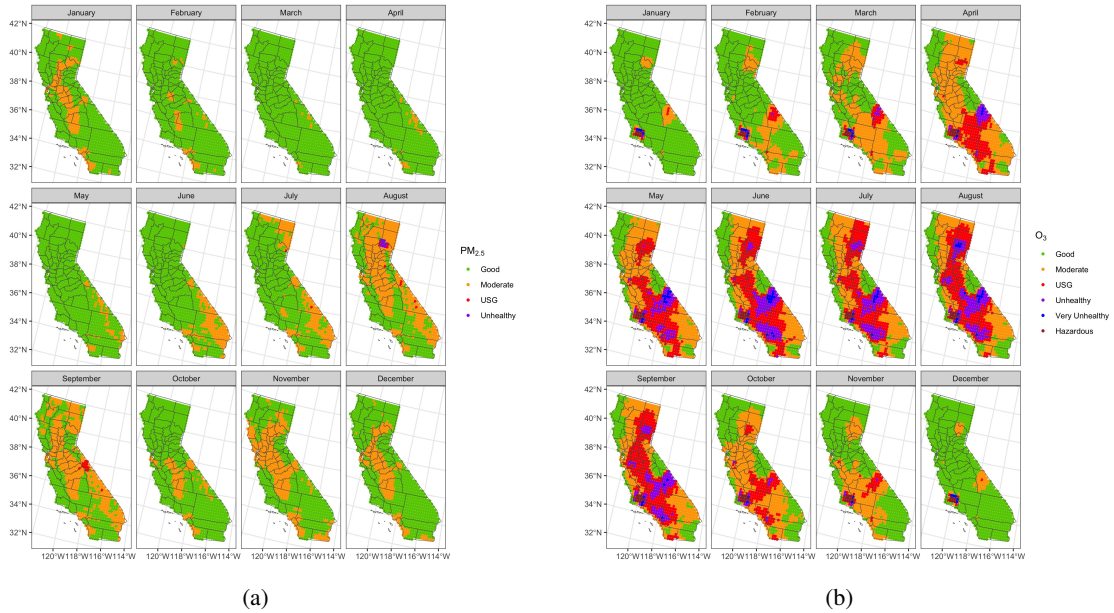


Figure 6: Prediction of monthly mean PM<sub>2.5</sub> (a) and monthly max ozone (b) over the entire California from January to December, 2021 based on Model 3.

spatial distribution, northern California appears to be more susceptible to experiencing moderate to unhealthy levels of PM<sub>2.5</sub>, while southern California is more likely to experience extreme levels of ozone pollution sustainably. It is noteworthy that the area around the intersection of San Luis Obispo

and Santa Barbara counties consistently exhibit maximum ozone levels exceeding the hazardous threshold throughout the year.

In air pollution research, of key is to identify regions with high pollution levels and predict air pollution patterns. These methods help visualize air quality conditions for the public and environmental regulators. The positive  $E_{u,\alpha}^+(X)$  and negative  $E_{u,\alpha}^-(X)$  excursion sets, proposed by Bolin and Lindgren (2015), determine the largest sets that simultaneously exceed or fall below the risk level  $u$  with a small error probability  $\alpha$ , utilizing a parametric family in conjunction with a sequential importance sampling technique to estimate joint probability distributions. To visualize the excursion sets simultaneously, we apply the positive and negative excursion functions,  $F_u^+(s) = 1 - \inf \{ \alpha \mid s \in E_{u,\alpha}^+ \}$  and  $F_u^-(s) = 1 - \inf \{ \alpha \mid s \in E_{u,\alpha}^- \}$ . The term  $\inf \{ \alpha \mid s_0 \in E_{u,\alpha}^+ \}$  denotes the "smallest"  $\alpha$  required for the location  $s_0$  to be included into the positive excursion set  $E_{u,\alpha}^+$ , while the higher  $1 - \inf \{ \alpha \mid s_0 \in E_{u,\alpha}^+ \}$  reported by positive excursion function generally indicates higher confidence/likelihood for the location  $s_0$  to exceed the risk threshold  $u$  simultaneously.

We set  $\alpha = 0.05$  and present in Fig. 7 for the positive excursion function with  $u = 71$  ppb and the negative excursion function with  $u = 54$  ppb. The two risk levels denote the cut-offs for 'Unhealthy for sensitive groups' and 'Good' categories for ozone concentrations, respectively. We see from Fig. 7(a) that, there is a consistently high probability for a set of areas with unhealthy ozone levels for sensitive populations, including San Luis Obispo and Santa Barbara counties. Additionally, the middle part of California are also prone to unhealthy ozone concentrations from May to October. Fig. 7(b) presents the areas considered relatively 'safe' concerning poor ozone air quality. More areas in winter maintain healthy  $O_3$  quality simultaneously than in the summer. Areas around the

intersection of Mono, Fresno and Inyo are likely to display good O<sub>3</sub> quality aligning with other parts of the state throughout the year.

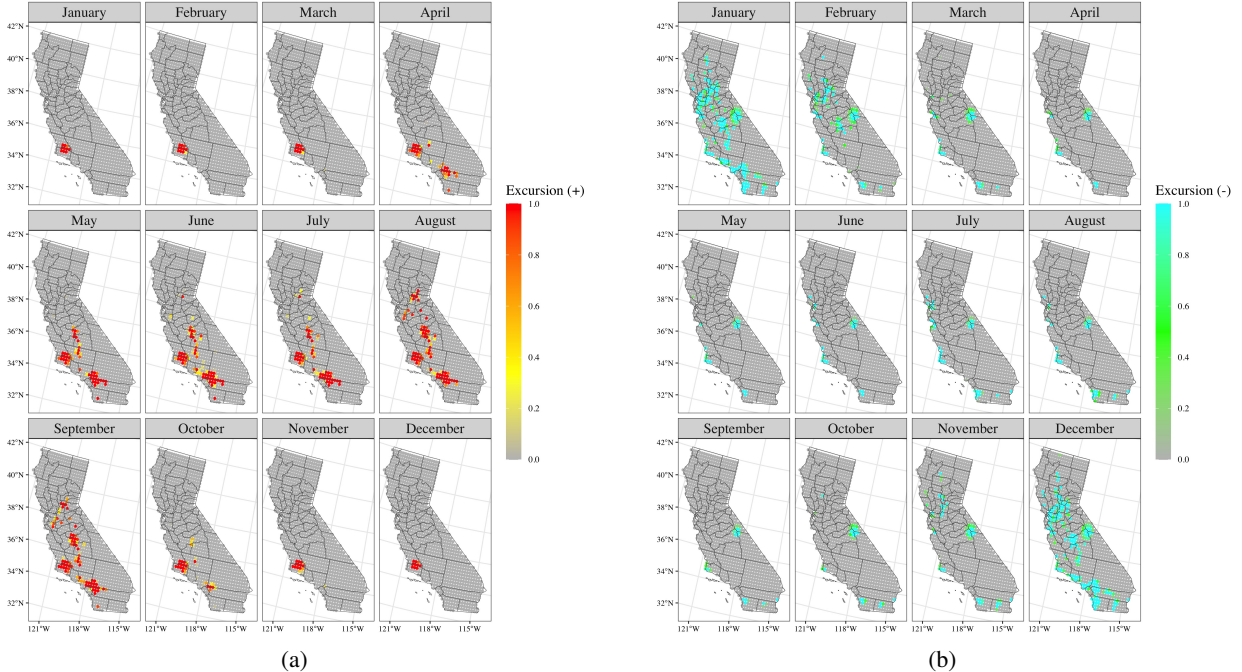


Figure 7: Positive and negative excursion functions of monthly maximum ozone from January to December in 2021, respectively. Here the thresholds for positive excursion function in (a) and negative excursion function in (b) are respectively 71 ppb and 54 ppb, indicating the "Unhealthy for sensitive groups" and "Good" categories of ozone according to the EPA in the U.S.

## 5 Discussion and conclusion

We proposed a joint spatio-temporal framework allowing for sharing stochastic interactions between extreme O<sub>3</sub> and moderate PM<sub>2.5</sub>. While the moderate PM<sub>2.5</sub> concentrations are (marginally) modelled using a log-Gaussian random field, the extreme O<sub>3</sub> levels are well fitted by the log-Gumbel model from extreme value theory. The high flexibility of our new models suggests that they can be more generally utilized to jointly model multiple processes in other contexts, e.g., extreme climate and environmental events as well as multiple interrelated diseases.

Our joint spatio-temporal Bayesian hierarchical model identified common and different drivers of the cumulative effect of  $\text{PM}_{2.5}$  and the extreme effect of  $\text{O}_3$  in California, providing new insights into the direction and magnitude of common drivers. The common drivers of temperature, extreme drought, fire burnt area and wind speed display significant influence on extreme  $\text{O}_3$  with less uncertainty than that on  $\text{PM}_{2.5}$ . The corresponding findings are consistent with those identified by Schnell and Prather (2017); Wang et al. (2017); Kalashnikov et al. (2022). As suggested by Chen et al. (2020), the inner causal effect of wind (i.e., wind directions together with speeds) and air pollutants can be further investigated. To conclude, our result demonstrated the improved inferences through sharing in our air pollution modelling. Similar advantages of joint sharing modelling are illustrated in the study of air pollution (Wang et al., 2023), wildfire (Koh et al., 2023; Zhang et al., 2023), landslides (Yadav et al., 2023) and disease (Alahmadi et al., 2024).

The joint  $\text{PM}_{2.5}$ - $\text{O}_3$  model provides new insights into appropriate risk controls and region-specified strategies.

- First, the reverse spatio-temporal interaction is demonstrated with a significant negative scaling coefficient, This discovery highlights the potential distinct spatio-temporal patterns of  $\text{PM}_{2.5}$  and ozone in California. Similar findings were identified by Jia et al. (2017) in East China. In addition, the peaks of  $\text{PM}_{2.5}$  and ozone appear respectively in cold and hot seasons, which is in correspondence with the observed inverse association between these two pollutants. Specifically, as shown by Jia et al. (2017), elevated  $\text{O}_3$  levels in hot season might stimulate the formation of secondary particles. In contrast, during the cold season,  $\text{PM}_{2.5}$  is likely to suppress surface solar radiation, thereby weaken  $\text{O}_3$  production.

- Second, the Bayesian framework of our joint continuous-time spatio-temporal models enables us to predict air pollutant conditions individually and identify hot-spots using excursion functions (for ozone) throughout the whole California. Our results suggest more attention to controlling serious  $PM_{2.5}$  and  $O_3$  pollution in the middle and north of California, respectively. Meanwhile, relevant agencies need to take seasonal actions when it comes to higher  $PM_{2.5}$  concentration in both autumn and winter and  $O_3$  in summer. Further, in the aid of excursion functions, the identified area around intersection of San Luis Obispo and Santa Barbara counties is likely to exceed simultaneously the unhealthy  $O_3$  level for sensitive population throughout the year. These findings not only enhance our understanding of air pollution dynamics but also serve as valuable insights for future policy making and resources allocation regarding the prevention and treatment of air pollution.

To conclude, we have implemented a novel joint Bayesian spatio-temporal model for multiple air pollutants, with shared random effects to account for stochastic dependence among different model components not explained by covariates. Different sharing strategies should be incorporated for different considerations (Koh et al., 2023). In this study, we emphasized on accurate inference of extreme ozone for its large spatial and temporal disparities. Our findings improve decision support in the co-control of  $PM_{2.5}$  and ozone at spatial scale. Future work could better explore both linear and non-linear effects of covariates by stochastic splines (Alahmadi et al., 2024).

## References

Ainsworth, E. A., Yendrek, C. R., Sitch, S., Collins, W. J., and Emberson, L. D. (2012). The effects of tropospheric ozone on net primary productivity and implications for climate change. *Annual review of plant biology*, 63:637–661.



- Akbari, M., Samadzadegan, F., and Weibel, R. (2015). A generic regional spatio-temporal co-occurrence pattern mining model: a case study for air pollution. *Journal of Geographical Systems*, 17:249–274.
- Alahmadi, H., van Niekerk, J., Padellini, T., and Rue, H. (2024). Joint quantile disease mapping with application to malaria and G6PD deficiency. *Royal Society Open Science*, 11(1):230851.
- American Lung Association (2023). State of the Air. Available online at <https://www.lung.org/research/sota/city-rankings/most-polluted-cities> (Accessed: February 16 2024).
- Amin, N. A. M., Adam, M. B., and Aris, A. Z. (2015). Bayesian extreme for modeling high PM<sub>10</sub> concentration in Johor. *Procedia Environmental Sciences*, 30:309–314.
- Arshinova, V., Belan, B., Lapchenko, V., Lapchenko, E., Rasskazchikova, T., Savkin, D., Sklyadneva, T., Tolmachev, G., and Fofonov, A. (2019). Changes in surface ozone concentration during precipitation. *Atmospheric and Oceanic Optics*, 32:671–679.
- Bell, M. L., Dominici, F., Ebisu, K., Zeger, S. L., and Samet, J. M. (2007). Spatial and temporal variation in PM<sub>2.5</sub> chemical composition in the united states for health effects studies. *Environmental Health Perspectives*, 115(7):989–995.
- Beloconi, A., Chrysoulakis, N., Lyapustin, A., Utzinger, J., and Vounatsou, P. (2018). Bayesian geostatistical modelling of PM<sub>10</sub> and PM<sub>2.5</sub> surface level concentrations in Europe using high-resolution satellite-derived products. *Environment International*, 121:57–70.
- Blangiardo, M., Cameletti, M., Baio, G., and Rue, H. (2013). Spatial and spatio-temporal models with R-INLA. *Spatial and Spatio-temporal Epidemiology*, 7:39–55.

- Bolin, D. and Lindgren, F. (2015). Excursion and contour uncertainty regions for latent Gaussian models. *Journal of the Royal Statistical Society Series B: Statistical Methodology*, 77(1):85–106.
- Bolin, D. and Wallin, J. (2023). Local scale invariance and robustness of proper scoring rules. *Statistical Science*, 38(1):140–159.
- Cameletti, M., Gómez-Rubio, V., and Blangiardo, M. (2019). Bayesian modelling for spatially misaligned health and air pollution data through the inla-spde approach. *Spatial Statistics*, 31:100353.
- Cameletti, M., Lindgren, F., Simpson, D., and Rue, H. (2013). Spatio-temporal modeling of particulate matter concentration through the SPDE approach. *AStA Advances in Statistical Analysis*, 97:109–131.
- Cao, B. and Yin, Z. (2020). Future atmospheric circulations benefit ozone pollution control in Beijing-Tianjin-Hebei with global warming. *Science of The Total Environment*, 743:140645.
- Castro-Camilo, D., Huser, R., and Rue, H. (2022). Practical strategies for generalized extreme value-based regression models for extremes. *Environmetrics*, 33(6):e2742.
- Chaudhuri, S., Saez, M., Varga, D., and Juan, P. (2023). Spatiotemporal modeling of traffic risk mapping: A study of urban road networks in barcelona, spain. *Spatial Statistics*, 53:100722.
- Chen, H.-C., Putra, K. T., Weng, C.-E., and Lin, J. C.-W. (2022). A novel predictor for exploring PM2.5 spatiotemporal propagation by using convolutional recursive neural networks. *Journal of Internet Technology*, 23(1):165–176.
- Chen, X., Shao, S., Tian, Z., Xie, Z., and Yin, P. (2017). Impacts of air pollution and its spatial spillover effect on public health based on China’s big data sample. *Journal of cleaner production*, 142:915–925.

- Chen, Z., Li, R., Chen, D., Zhuang, Y., Gao, B., Yang, L., and Li, M. (2020). Understanding the causal influence of major meteorological factors on ground ozone concentrations across China. *Journal of Cleaner Production*, 242:118498.
- Coles, S., Bawa, J., Trenner, L., and Dorazio, P. (2001). *An introduction to statistical modeling of extreme values*. Springer.
- Craig, L., Brook, J. R., Chiotti, Q., Croes, B., Gower, S., Hedley, A., Krewski, D., Krupnick, A., Krzyzanowski, M., Moran, M. D., et al. (2008). Air pollution and public health: a guidance document for risk managers. *Journal of Toxicology and Environmental Health, Part A*, 71(9-10):588–698.
- Dai, H., Zhu, J., Liao, H., Li, J., Liang, M., Yang, Y., and Yue, X. (2021). Co-occurrence of ozone and PM<sub>2.5</sub> pollution in the Yangtze River Delta over 2013–2019: Spatiotemporal distribution and meteorological conditions. *Atmospheric Research*, 249:105363.
- De Hoogh, K., Chen, J., Gulliver, J., Hoffmann, B., Hertel, O., Ketzel, M., Bauwelinck, M., van Donkelaar, A., Hvidtfeldt, U. A., Katsouyanni, K., et al. (2018). Spatial PM<sub>2.5</sub>, NO<sub>2</sub>, O<sub>3</sub> and BC models for Western Europe–Evaluation of spatiotemporal stability. *Environment International*, 120:81–92.
- Dias, D. and Tchepel, O. (2018). Spatial and temporal dynamics in air pollution exposure assessment. *International journal of environmental research and public health*, 15(3):558.
- Ebi, K. L. and McGregor, G. (2008). Climate change, tropospheric ozone and particulate matter, and health impacts. *Environmental Health Perspectives*, 116(11):1449–1455.
- Embrechts, P., Klüppelberg, C., and Mikosch, T. (2013). *Modelling extremal events: for insurance and finance*. Springer Science & Business Media.

- Fang, X., Li, R., Xu, Q., Bottai, M., Fang, F., and Cao, Y. (2016). A two-stage method to estimate the contribution of road traffic to PM<sub>2.5</sub> concentrations in Beijing, China. *International Journal of Environmental Research and Public Health*, 13(1):124.
- Fioravanti, G., Martino, S., Cameletti, M., and Cattani, G. (2021). Spatio-temporal modelling of PM<sub>10</sub> daily concentrations in Italy using the SPDE approach. *Atmospheric Environment*, 248:118192.
- Forlani, C., Bhatt, S., Cameletti, M., Krainski, E., and Blangiardo, M. (2020). A joint bayesian space–time model to integrate spatially misaligned air pollution data in R-INLA. *Environmetrics*, 31(8):e2644.
- Fuglstad, G.-A., Simpson, D., Lindgren, F., and Rue, H. (2019). Constructing priors that penalize the complexity of Gaussian random fields. *Journal of the American Statistical Association*, 114(525):445–452.
- Gardner-Frolick, R., Boyd, D., and Giang, A. (2022). Selecting data analytic and modeling methods to support air pollution and environmental justice investigations: a critical review and guidance framework. *Environmental Science & Technology*, 56(5):2843–2860.
- Gelman, A., Hwang, J., and Vehtari, A. (2014). Understanding predictive information criteria for Bayesian models. *Statistics and computing*.
- Gneiting, T. and Raftery, A. E. (2007). Strictly proper scoring rules, prediction, and estimation. *Journal of the American Statistical Association*, 102(477):359–378.
- Gold, D. R., Damokosh, A. I., Pope III, C. A., Dockery, D. W., McDonnell, W. F., Serrano, P., Retama, A., and Castillejos, M. (1999). Particulate and ozone pollutant effects on the respiratory function of children in southwest Mexico City. *Epidemiology*, 10(1):8–16.

- Gouldsbrough, L., Hossaini, R., Eastoe, E., and Young, P. J. (2022). A temperature dependent extreme value analysis of UK surface ozone, 1980–2019. *Atmospheric Environment*, 273:118975.
- Guan, W.-J., Zheng, X.-Y., Chung, K. F., and Zhong, N.-S. (2016). Impact of air pollution on the burden of chronic respiratory diseases in China: time for urgent action. *The Lancet*.
- Guan, Y., Xiao, Y., Wang, Y., Zhang, N., and Chu, C. (2021). Assessing the health impacts attributable to PM<sub>2.5</sub> and ozone pollution in 338 Chinese cities from 2015 to 2020. *Environmental Pollution*, 287:117623.
- Hao, Y., Balluz, L., Strosnider, H., Wen, X. J., Li, C., and Qualters, J. R. (2015). Ozone, fine particulate matter, and chronic lower respiratory disease mortality in the United States. *American Journal of Respiratory and Critical Care Medicine*, 192(3):337–341.
- Huang, L., Sun, J., Jin, L., Brown, N. J., and Hu, J. (2021). Strategies to reduce PM<sub>2.5</sub> and O<sub>3</sub> together during late summer and early fall in San Joaquin Valley, California. *Atmospheric Research*, 258:105633.
- Jaffe, D. A. and Wigder, N. L. (2012). Ozone production from wildfires: a critical review. *Atmospheric Environment*, 51:1–10.
- Jerrett, M., Burnett, R. T., Beckerman, B. S., Turner, M. C., Krewski, D., Thurston, G., Martin, R. V., van Donkelaar, A., Hughes, E., Shi, Y., et al. (2013). Spatial analysis of air pollution and mortality in California. *American Journal of Respiratory and Critical Care Medicine*, 188(5):593–599.
- Jia, M., Zhao, T., Cheng, X., Gong, S., Zhang, X., Tang, L., Liu, D., Wu, X., Wang, L., and Chen, Y. (2017). Inverse relations of PM<sub>2.5</sub> and O<sub>3</sub> in air compound pollution between cold and hot seasons over an urban area of East China. *Atmosphere*, 8(3).

- Kalashnikov, D. A., Schnell, J. L., Abatzoglou, J. T., Swain, D. L., and Singh, D. (2022). Increasing co-occurrence of fine particulate matter and ground-level ozone extremes in the western United States. *Science Advances*, 8(1):eabi9386.
- Karambelas, A., Holloway, T., Kinney, P. L., Fiore, A. M., DeFries, R., Kieseewetter, G., and Heyes, C. (2018). Urban versus rural health impacts attributable to PM<sub>2.5</sub> and O<sub>3</sub> in northern india. *Environmental Research Letters*, 13(6):064010.
- Kaufman, J. D., Elkind, M. S., Bhatnagar, A., Koehler, K., Balmes, J. R., Sidney, S., Burroughs Peña, M. S., Dockery, D. W., Hou, L., Brook, R. D., et al. (2020). Guidance to reduce the cardiovascular burden of ambient air pollutants: a policy statement from the American Heart Association. *Circulation*, 142(23):e432–e447.
- Kinney, P. L. (2018). Interactions of climate change, air pollution, and human health. *Current Environmental Health Reports*, 5:179–186.
- Koh, J., Pimont, F., Dupuy, J.-L., and Opitz, T. (2023). Spatiotemporal wildfire modeling through point processes with moderate and extreme marks. *The Annals of Applied Statistics*, 17(1):560–582.
- Lenox, M. J. and Haines, Y. Y. (1996). The constrained extremal distribution selection method. *Risk analysis*.
- Lewis, P. O., Xie, W., Chen, M.-H., Fan, Y., and Kuo, L. (2014). Posterior predictive Bayesian phylogenetic model selection. *Systematic Biology*, 63(3):309–321.
- Li, L., Li, Q., Huang, L., Wang, Q., Zhu, A., Xu, J., Liu, Z., Li, H., Shi, L., Li, R., et al. (2020). Air quality changes during the covid-19 lockdown over the yangtze river delta region: An insight

- into the impact of human activity pattern changes on air pollution variation. *Science of the Total Environment*, 732:139282.
- Li, S. and Banerjee, T. (2021). Spatial and temporal pattern of wildfires in California from 2000 to 2019. *Scientific Reports*, 11(1):8779.
- Lim, C.-H., Ryu, J., Choi, Y., Jeon, S. W., and Lee, W.-K. (2020). Understanding global PM<sub>2.5</sub> concentrations and their drivers in recent decades (1998–2016). *Environment International*, 144:106011.
- Lindgren, F., Rue, H., and Lindström, J. (2011). An explicit link between Gaussian fields and Gaussian Markov random fields: the stochastic partial differential equation approach. *Journal of the Royal Statistical Society Series B: Statistical Methodology*, 73(4):423–498.
- Lindström, J., Szpiro, A. A., Sampson, P. D., Oron, A. P., Richards, M., Larson, T. V., and Sheppard, L. (2014). A flexible spatio-temporal model for air pollution with spatial and spatio-temporal covariates. *Environmental and Ecological Statistics*, 21:411–433.
- Liu, N., Lin, W., Ma, J., Xu, W., and Xu, X. (2019). Seasonal variation in surface ozone and its regional characteristics at global atmosphere watch stations in China. *Journal of Environmental Sciences*, 77:291–302.
- Lu, J. G. (2020). Air pollution: A systematic review of its psychological, economic, and social effects. *Current opinion in psychology*, 32:52–65.
- Malig, B. J., Pearson, D. L., Chang, Y. B., Broadwin, R., Basu, R., Green, R. S., and Ostro, B. (2016). A time-stratified case-crossover study of ambient ozone exposure and emergency department visits for specific respiratory diagnoses in California (2005–2008). *Environmental Health Perspectives*, 124(6):745–753.

- Martino, S. and Riebler, A. (2019). Integrated Nested Laplace approximations (INLA). *arXiv preprint arXiv:1907.01248*.
- Martins, L. D., Wikuats, C. F. H., Capucim, M. N., de Almeida, D. S., da Costa, S. C., Albuquerque, T., Carvalho, V. S. B., de Freitas, E. D., de Fátima Andrade, M., and Martins, J. A. (2017). Extreme value analysis of air pollution data and their comparison between two large urban regions of South America. *Weather and Climate Extremes*, 18:44–54.
- McCormick, N. J. (1981). *Reliability and risk analysis: Methods and nuclear power applications*. Academic Press.
- Mekonnen, Z. K., Oehlert, J. W., Eskenazi, B., Shaw, G. M., Balmes, J. R., and Padula, A. M. (2021). The relationship between air pollutants and maternal socioeconomic factors on preterm birth in California urban counties. *Journal of Exposure Science & Environmental Epidemiology*, 31(3):503–513.
- Meo, S. A., Abukhalaf, A. A., Alomar, A. A., Alessa, O. M., Sami, W., and Klonoff, D. C. (2021). Effect of environmental pollutants PM<sub>2.5</sub>, carbon monoxide, and ozone on the incidence and mortality of SARS-COV-2 infection in ten wildfire affected counties in California. *Science of the Total Environment*, 757:143948.
- Minasny, B. and McBratney, A. B. (2007). Spatial prediction of soil properties using EBLUP with the Matérn covariance function. *Geoderma*, 140(4):324–336.
- Moraga, P. (2019). *Geospatial health data: Modeling and visualization with R-INLA and shiny*. CRC Press.
- Murray, C. J., Aravkin, A. Y., Zheng, P., Abbafati, C., Abbas, K. M., Abbasi-Kangevari, M., Abd-Allah, F., Abdelalim, A., Abdollahi, M., Abdollahpour, I., et al. (2020). Global burden of



- 87 risk factors in 204 countries and territories, 1990–2019: a systematic analysis for the global burden of disease study 2019. *The Lancet*, 396(10258):1223–1249.
- Muñoz Sabater, J. (2019a). ERA5-Land hourly data from 1950 to present. Copernicus Climate Change Service (C3S) Climate Data Store (CDS). DOI: 10.24381/cds.e2161bac. Accessed: July 16 2024.
- Muñoz Sabater, J. (2019b). ERA5-Land monthly averaged data from 1950 to present. Copernicus Climate Change Service (C3S) Climate Data Store (CDS). DOI: 10.24381/cds.68d2bb30. Accessed: January 16 2024.
- Nuvolone, D., Petri, D., and Voller, F. (2018). The effects of ozone on human health. *Environmental Science and Pollution Research*, 25:8074–8088.
- Nychka, D., Wikle, C., and Royle, J. A. (2002). Multiresolution models for nonstationary spatial covariance functions. *Statistical Modelling*, 2(4):315–331.
- Opitz, T., Bonneau, F., and Gabriel, E. (2020). Point-process based bayesian modeling of space–time structures of forest fire occurrences in mediterranean france. *Spatial Statistics*, 40:100429.
- Opitz, T., Huser, R., Bakka, H., and Rue, H. (2018). Inla goes extreme: Bayesian tail regression for the estimation of high spatio-temporal quantiles. *Extremes*, 21(3):441–462.
- O’Dell, K., Ford, B., Fischer, E. V., and Pierce, J. R. (2019). Contribution of wildland-fire smoke to US PM<sub>2.5</sub> and its influence on recent trends. *Environmental Science & Technology*, 32(4):1797–1804.
- Pisarenko, V., Sornette, A., Sornette, D., and Rodkin, M. (2014). Characterization of the tail of the distribution of earthquake magnitudes by combining the gev and gpd descriptions of extreme value theory. *Pure and Applied Geophysics*, 171:1599–1624.

- Rhee, J., Dominici, F., Zanobetti, A., Schwartz, J., Wang, Y., Di, Q., Balmes, J., and Christiani, D. C. (2019). Impact of long-term exposures to ambient PM<sub>2.5</sub> and ozone on ARDS risk for older adults in the United States. *Chest*, 156(1):71–79.
- Righetto, A. J., Faes, C., Vandendijck, Y., and Ribeiro, P. J. (2020). On the choice of the mesh for the analysis of geostatistical data using R-INLA. *Communications in Statistics - Theory and Methods*, 49(1):203–220.
- Rue, H., Martino, S., and Chopin, N. (2009). Approximate Bayesian inference for latent Gaussian models by using integrated nested Laplace approximations. *Journal of the Royal Statistical Society Series B: Statistical Methodology*, 71:319–392.
- Rulfova, Z., Buishand, A., Roth, M., and Kysely, J. (2016). A two-component generalized extreme value distribution for precipitation frequency analysis. *Journal of Hydrology*, 534:659–668.
- Salmeron, R., Garcıa, C., and Garcıa, J. (2018). Variance inflation factor and condition number in multiple linear regression. *Journal of Statistical Computation and Simulation*, 88(12):2365–2384.
- Schnell, J. L. and Prather, M. J. (2017). Co-occurrence of extremes in surface ozone, particulate matter, and temperature over eastern North America. *Proceedings of the National Academy of Sciences*, 114(11):2854–2859.
- Service, C. C. C. and Store, C. D. (2019). Fire burned area from 2001 to present derived from satellite observation. Fire burned area from 2001 to present derived from satellite observation. DOI: 10.24381/cds.f333cf85. Accessed: July 16 2024.
- Shcherbakov, R., Zhuang, J., Zoller, G., and Ogata, Y. (2019). Forecasting the magnitude of the largest expected earthquake. *Nature Communications*, 10(1):4051.

- Shi, L., Zanobetti, A., Kloog, I., Coull, B. A., Koutrakis, P., Melly, S. J., and Schwartz, J. D. (2016). Low-concentration PM<sub>2.5</sub> and mortality: estimating acute and chronic effects in a population-based study. *Environmental Health Perspectives*, 124(1):46–52.
- Sicard, P., Agathokleous, E., De Marco, A., Paoletti, E., and Calatayud, V. (2021). Urban population exposure to air pollution in Europe over the last decades. *Environmental Sciences Europe*, 33(1):1–12.
- Siddika, N., Rantala, A. K., Antikainen, H., Balogun, H., Amegah, A. K., Ryti, N. R., Kukkonen, J., Sofiev, M., Jaakkola, M. S., and Jaakkola, J. J. (2019). Synergistic effects of prenatal exposure to fine particulate matter (PM<sub>2.5</sub>) and ozone (O<sub>3</sub>) on the risk of preterm birth: a population-based cohort study. *Environmental Research*, 176:108549.
- Sillmann, J., Thorarinsdottir, T., Keenlyside, N., Schaller, N., Alexander, L. V., Hegerl, G., Seneviratne, S. I., Vautard, R., Zhang, X., and Zwiers, F. W. (2017). Understanding, modeling and predicting weather and climate extremes: Challenges and opportunities. *Weather and climate extremes*, 18:65–74.
- Simpson, D., Rue, H., Riebler, A., Martins, T. G., and Sørbye, S. H. (2017). Penalising model component complexity: A principled, practical approach to constructing priors. *Statistical Science*, 32(1):1–28.
- Spiegelhalter, D. J., Best, N. G., Carlin, B. P., and Van Der Linde, A. (2002). Bayesian measures of model complexity and fit. *Journal of the Royal Statistical Society: Series B: Statistical Methodology*, 64(4):583–639.
- Tai, A. P., Mickley, L. J., and Jacob, D. J. (2010). Correlations between fine particulate matter (PM<sub>2.5</sub>) and meteorological variables in the United States: Implications for the sensitivity of PM<sub>2.5</sub> to

climate change. *Atmospheric environment*.

Tingey, D. T. et al. (1984). The co-occurrence of potentially phytotoxic concentrations of various gaseous air pollutants. *Atmospheric Environment (1967)*, 18(11):2521–2526.

Vandeskog, S., Martino, S., Castro-Camilo, D., and Rue, H. (2022). Modelling sub-daily precipitation extremes with the blended generalised extreme value distribution. *Journal of Agricultural, Biological and Environmental Statistics*, 27:598–621.

Vehtari, A. et al. (2021). Widely applicable information criterion (WAIC).

Vettori, S., Huser, R., and Genton, M. G. (2019). Bayesian modeling of air pollution extremes using nested multivariate max-stable processes. *Biometrics*, 75(3):831–841.

Vicedo-Cabrera, A. M., Sera, F., Liu, C., Armstrong, B., Milojevic, A., Guo, Y., Tong, S., Lavigne, E., Kyselý, J., Urban, A., et al. (2020). Short term association between ozone and mortality: global two stage time series study in 406 locations in 20 countries. *British Medical Journal*, 368.

Villejo, S. J., Illian, J. B., and Swallow, B. (2023). Data fusion in a two-stage spatio-temporal model using the inla-spde approach. *Spatial Statistics*, 54:100744.

Wang, K., Ling, C., Chen, Y., and Zhang, Z. (2023). Spatio-temporal joint modelling on moderate and extreme air pollution in Spain. *Environmental and Ecological Statistics*, 30(1):601–624.

Wang, M., Sampson, P. D., Hu, J., Kleeman, M., Keller, J. P., Olives, C., Szpiro, A. A., Vedal, S., and Kaufman, J. D. (2016). Combining land-use regression and chemical transport modeling in a spatiotemporal geostatistical model for ozone and PM<sub>2.5</sub>. *Environmental Science & Technology*, 50(10):5111–5118.

Wang, P., Chen, K., Zhu, S., Wang, P., and Zhang, H. (2020). Severe air pollution events not avoided by reduced anthropogenic activities during COVID-19 outbreak. *Resources, Conservation and*

- Recycling*, 158:104814.
- Wang, Y., Xie, Y., Dong, W., Ming, Y., Wang, J., and Shen, L. (2017). Adverse effects of increasing drought on air quality via natural processes. *Atmospheric Chemistry and Physics*, 17(20):12827–12843.
- Watanabe, S. (2010). Asymptotic equivalence of Bayes cross validation and widely applicable information criterion in singular learning theory. *Journal of Machine Learning Research*, 11:3571–3594.
- Weber, S. A., Insaf, T. Z., Hall, E. S., Talbot, T. O., and Huff, A. K. (2016). Assessing the impact of fine particulate matter (PM<sub>2.5</sub>) on respiratory-cardiovascular chronic diseases in the New York City metropolitan area using hierarchical Bayesian model estimates. *Environmental Research*, 151:399–409.
- Wong, C.-M., Vichit-Vadakan, N., Kan, H., and Qian, Z. (2008). Public health and air pollution in asia (papa): a multicity study of short-term effects of air pollution on mortality. *Environmental Health Perspectives*, 116(9):1195–1202.
- Xu, G., Ren, X., Xiong, K., Li, L., Bi, X., and Wu, Q. (2020). Analysis of the driving factors of PM<sub>2.5</sub> concentration in the air: A case study of the Yangtze River Delta, China. *Ecological Indicators*, 110:105889.
- Yadav, R., Huser, R., Opitz, T., and Lombardo, L. (2023). Joint modelling of landslide counts and sizes using spatial marked point processes with sub-asymptotic mark distributions. *Journal of the Royal Statistical Society Series C: Applied Statistics*, 72(5):1139–1161.
- Zhang, Q. and Geng, G. (2019). Impact of clean air action on PM<sub>2.5</sub> pollution in China. *Science China Earth Sciences*.

Zhang, Z., Krainski, E., Zhong, P., Rue, H., and Huser, R. (2023). Joint modeling and prediction of massive spatio-temporal wildfire count and burnt area data with the INLA-SPDE approach.

*Extremes*, 26(2):339–351.

Zhou, Y., Chang, F.-J., Chen, H., and Li, H. (2020). Exploring copula-based Bayesian model averaging with multiple ANNs for PM<sub>2.5</sub> ensemble forecasts. *Journal of Cleaner Production*,

263:121528.

Zhu, S., Horne, J. R., Mac Kinnon, M., Samuelsen, G., and Dabdub, D. (2019). Comprehensively assessing the drivers of future air quality in California. *Environment International*.